Laboratory characterization of a "Foucault-like" wavefront sensor for Adaptive Optics

A. Riccardi[a], N. Bindi[b], R. Ragazzoni[c], S. Esposito[a] and P. Stefanini[a]

[a]Osservatorio Astrofisico di Arcetri, Largo E. Fermi 5, 50125 Firenze, Italy

[b]Dipartimento di Astronomia e Scienza dello Spazio, Largo E. Fermi 5, , 50125 Firenze, Italy

[c]Osservatorio Astronomico di Padova, Vicolo dell'Osservatorio 5, 35122 Padova, Italy

ABSTRACT

We present a prototype of a Foucault-Like Wavefront Sensor (FLWS) that will be implemented in the Adaptive Optics Systems of 3.5m TNG and is one of the proposed choices for the 2x8.4m LBT. The FLWS has some interesting features for Adaptive Optics applications: it has a linear relationship between measured signals and wavefront derivatives like the Shack-Hartmann sensor, it allows to change on the fly the gain used for wavefront measurements like the Curvature Sensor, and finally it allows to modify easily the wavefront aberration spatial sampling. The developed prototype of the FLWS is described and first laboratory results are presented. Measurements of static wavefront aberrations performed by the FLWS and a Wyko interferometer are compared to test the accuracy of the sensor, giving an error of a few tens of nm in terms of reconstructed wavefront rms, when aberrations of typical atmospheric turbulence strength are induced.

Keywords: Adaptive optics, wavefront sensing

1. INTRODUCTION

The typical wavefront sensors used in astronomical adaptive optics systems are the Shack-Hartmann (SH) and the curvature ones, measuring the gradient and the Laplacian of the wavefront distortion respectively.

The SH sensor provides simple linear relationships between the measured quantity (the position of the spot produced by each lenslet) and the local wavefront gradient, but it has very low flexibility in terms of the possibility to optimize during the operation the pupil sampling and the gain (i.e. response vs. measured wavefront deformation). This is essentially due to the severe constrains arising from the lenslet array alignment. In this kind of device the sampling and gain are usually stated during the design phase, optimized for some average condition and cannot be modified.

The curvature sensor hasn't a linear relationship between the measured quantities (the out-of-focus intensity pattern) and the wavefront Laplacian. It also needs an estimation of the normal first derivative on the boundary of the pupil to reconstruct the wavefront. However it has the possibility to change the gain in a continuous mode modulating the amount of defocus used to retrieve the wavefront Laplacian[1] in order to operate in the linear regime and optimize the gain depending on the current status of the system.

The Foucault-Like Wavefront Sensor (FLWS) described in this paper was proposed for the first time by R. Ragazzoni,[2] it joins some advantages of the previous sensors and some new ones: it provides simple linear relationship between the measured signals and the first derivatives of the wavefront, and it can change easily the sampling and the gain during the operation, in order to optimize the behavior of the sensor depending on the correcting wavelength, the status of the adaptive correction, the seeing condition and brightness of the guide source.

The FLWS will be implemented in the 3.5 m Telescopio Nazionale Galileo (TNG) adaptive optics system[3] and is one of the proposed sensors for the 2x8.4 m Large binocular Telescope[4,5] (LBT) adaptive optics system. The

Other author information: (Send correspondence to A.R.)
A.R.: E-mail: riccardi@arcetri.astro.it
N.B.: E-mail: bindi@arcetri.astro.it
R.R.: E-mail: ragazzoni@pd.astro.it
S.E.: E-mail: esposito@arcetri.astro.it
P.S.: E-mail: stefanini@arcetri.astro.it

Part of the SPIE Conference on Adaptive Optical System Technologies • Kona, Hawaii • March 1998
SPIE Vol. 3353 • 0277-786X/98/$10.00

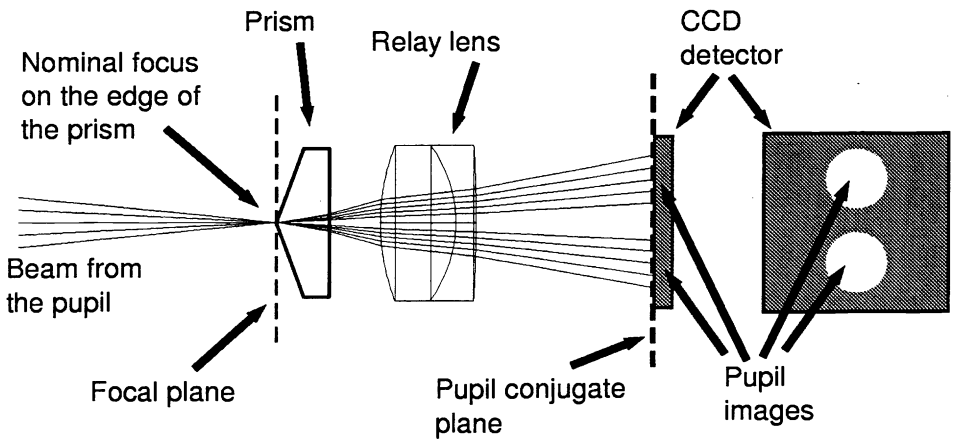

Figure 1. Foucault-like wavefront sensor (FLWS) essential components.

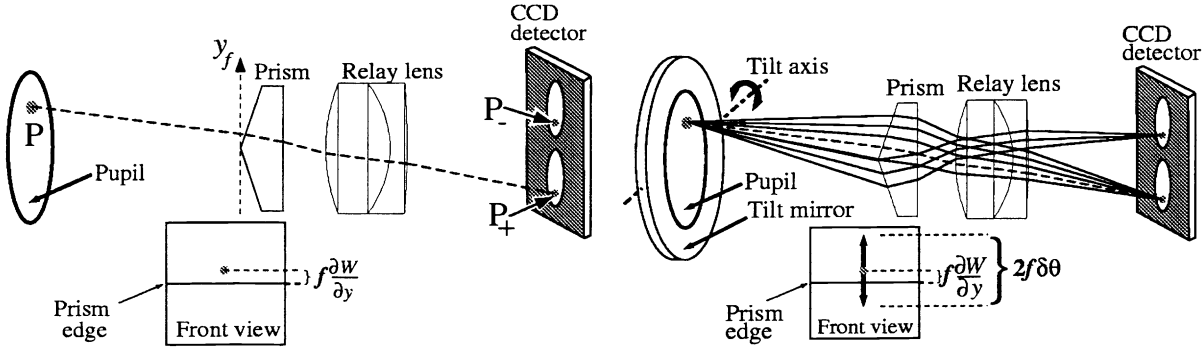

Figure 2. Principle of operation of the FLWS.

prototype of the FLWS located in Arcetri will be also used as a fast wavefront sensor for the optical laboratory dynamical tests of the P30 MMT prototype.[6–8]

The involved institutes in the development of the FLWS are the Observatories of Padova, Arcetri and Merate (Italy). The FLWS is also a research item in the European Community TMR network.

In the first part of the paper the principle of operation for the FLWS is described in detail pointing out its advantages and some specifications. In the second part we present the laboratory results obtained in Arcetri with a prototype of the sensor.

2. DESCRIPTION OF THE FOUCAULT-LIKE WAVEFRONT SENSOR

2.1. Principle of operation

In order to describe the principle of operation for the FLWS, we sketch a simplified configuration able to retrieve the derivative of the wavefront along only one direction. In this case, the essential components for the FLWS are shown in Fig. 1. The nominal focus point is set on the edge of a prism that splits the focused beam in two paths along along the orthogonal direction respect to the edge itself. Finally a relay lens placed behind the prism produces two images of the telescope pupil on a detector.

Assuming the geometrical optics regime is valid, if the ray originating from a generic point $P = (x, y)$ on the pupil plane is aberrated (see Fig. 2a), it doesn't reach the focus plane in the nominal focus point, but it is displaced from the prism edge by the quantity[9]

$$y_f = f\frac{\partial W}{\partial y}(x, y)\,, \tag{1}$$

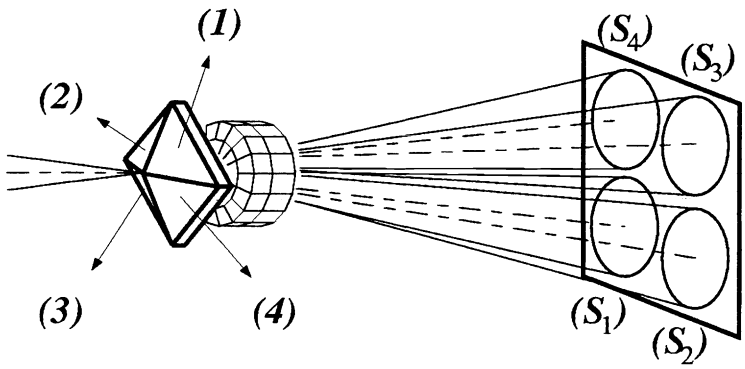

Figure 3. The pyramid splits the beam focused on its vertex in four beams generating four images of the pupil.

where (x_f, y_f) are the coordinates on the focus plane (with the x_f axis along the prism edge), f is the effective telescope focal length and $W(x,y)$ is the wavefront distortion pattern on the pupil plane. The ray is refracted towards only one of the two images of the pupil depending on the sign of $\frac{\partial W}{\partial y}(x,y)$. When the derivative is positive the ray originating from P reaches the conjugated point P_+ on the bottom pupil image, otherwise it reaches the conjugated point P_- on the top pupil image. In Fig. 2a, for instance, $\frac{\partial W}{\partial y}(P) > 0$ giving a bright region in P_+ and a completely dark region in P_-. In such a configuration it isn't possible to retrieve any information about the value of the derivative of the wavefront but its sign. It is only possible to obtain a qualitative estimation of the presence of some primary aberration by the shape of the dark-and-bright pattern on the image of the pupil (standard Foucault test[10]).

In order to obtain a quantitative estimation of the $\frac{\partial W}{\partial y}$ pattern using the Foucault test in the geometrical optics regime, some methods were proposed in literature,[11,12] but they are not useful for Adaptive Optics purposes because of the long time and the large number of frame acquisitions needed to restore a single wavefront. To overcome such problems, we can introduce an overall tilt oscillation on the pupil plane, setting, for instance, an image of the pupil on a tilting mirror somewhere in the beam before the prism. Letting $\delta\theta_y$ the angular amplitude of the tilt modulation in the orthogonal direction respect to the prism edge, and assuming

$$\delta\theta_y > \left| \frac{\partial W}{\partial y}(P) \right| , \tag{2}$$

the ray starts sweeping both the faces of the prism, as shown in Fig. 2b. After one period of the tilt modulation the signals S_+ and S_-, recorded by the detector in the points P_+ and P_-, are proportional to the transit time of the ray on the related face of the prism, hence the difference $S_+ - S_-$ is related to the displacement of the unmodulated ray from the edge. Assuming a linear angular modulation of the tilt respect to the time (*ramp modulation*), we obtain the following relation between the derivative and the signals

$$\frac{\partial W}{\partial y}(P) = \delta\theta_y \frac{S_+ - S_-}{S_+ + S_-} , \tag{3}$$

giving, for each frame acquisition, the estimation of the derivative along the y direction on the whole pupil. A similar equation can be obtain for $\frac{\partial W}{\partial x}$ if the prism is set with edge along the y_f axis.

2.2. The pyramid configuration

In order to obtain the pattern of $\frac{\partial W}{\partial x}$ and $\frac{\partial W}{\partial y}$ simultaneously, R. Ragazzoni proposed to use a pyramid with the vertex on the nominal focus point.[2] As shown in Fig. 3, the beam is split in four beams producing four images of the pupil. In this configuration the cross edge of the pyramid acts like two equivalent superimposed prisms with orthogonal edges, giving

$$S_+ = S_1 + S_2 \tag{4}$$
$$S_- = S_3 + S_4 , \tag{5}$$

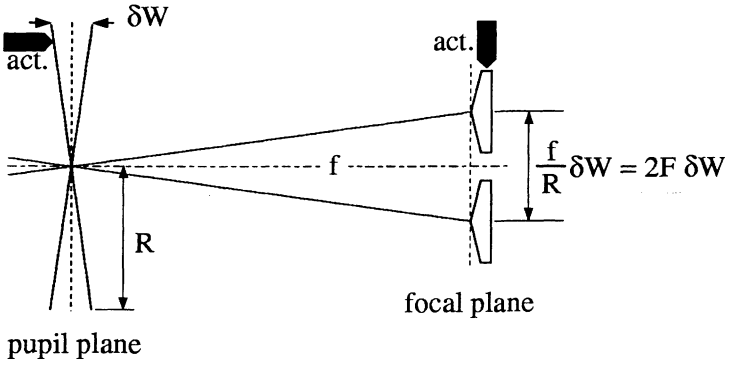

Figure 4. Comparison between the actuator stroke needed for the pupil (δW) and the equivalent focal plane tilt modulation ($\propto F\delta W$). R, f and F are the pupil radius, the effective focal length and the F-number respectively.

for the equivalent prism with the edge along the y_f axis and

$$S_+ = S_1 + S_4 \tag{6}$$
$$S_- = S_2 + S_3\,, \tag{7}$$

for the equivalent prism with the edge along the x_f axis. Using Eq. (3) we obtain the pyramid-case relations

$$\begin{aligned} \frac{\partial W}{\partial x} &= \delta\theta_x \frac{(S_1+S_4)-(S_2+S_3)}{S_1+S_2+S_3+S_4} \\ \frac{\partial W}{\partial y} &= \delta\theta_y \frac{(S_1+S_2)-(S_3+S_4)}{S_1+S_2+S_3+S_4}\,. \end{aligned} \tag{8}$$

The needed simultaneous oscillations along the x and y axis can be superimposed in phase. In this case only a one-axis tilt modulator is needed performing an oscillation along the 45 deg direction in the (x,y) plane ($\delta\theta_x = \delta\theta_y = \delta\theta$). A more compact and simple configuration for the sensor can be obtained eliminating the tilt mirror and the optics needed to produce the image of the pupil on it, because the tilt modulation can be obtained translating the pyramid itself with a displacement $f\delta\theta$.[2] This is the configuration that will be implemented in the TNG Adaptive Optics System. This kind of solution has only one drawback, it needs a modulator with the same bandpass, but a larger stroke, $\approx F$ times larger then in the previous case, where F is the F-number of the focussed beam, as shown in Fig. 4.

The ramp modulation produces large accelerations at the turning points and cannot be exactly reproduced because of the finite bandwidth of the oscillating system. This effect can be taken into account in the Eqs. 8, when the oscillation law is known. For instance, if a ***sinusoidal modulation*** is performed the Eqs. 8 becomes

$$\begin{aligned} \frac{\partial W}{\partial x} &= \delta\theta_x \sin\left[\frac{\pi}{2}\frac{(S_1+S_4)-(S_2+S_3)}{S_1+S_2+S_3+S_4}\right] \\ \frac{\partial W}{\partial y} &= \delta\theta_y \sin\left[\frac{\pi}{2}\frac{(S_1+S_2)-(S_3+S_4)}{S_1+S_2+S_3+S_4}\right]. \end{aligned} \tag{9}$$

2.3. Characteristics of the pyramid

Referring to the Fig. 5, the angular separation β between the axes of two beams split by two opposed faces of the pyramid is given by

$$\beta = (n-1)\alpha\,, \tag{10}$$

where α is the angle between the two faces, n is the refractive index of the pyramid glass and the small-angle-approximation is used for the Snell law. To avoid the overlapping of the split beams $\beta \geq \sqrt{2}/F$, where F is the F-number of the focused beam. For the best data packing configuration ($\beta = \sqrt{2}/F$), Eq. 10 states

$$\alpha = \frac{\sqrt{2}}{F(n-1)}\,, \tag{11}$$

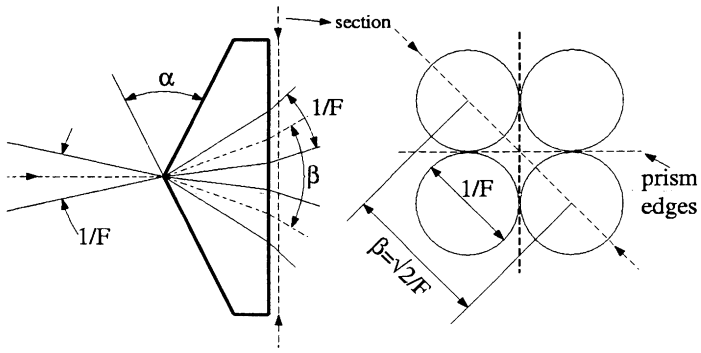

Figure 5. Geometry of the splitting effects of the pyramid. F represents the F-number of the beam focused on the pyramid vertex. The right figure represent the best data packing configuration.

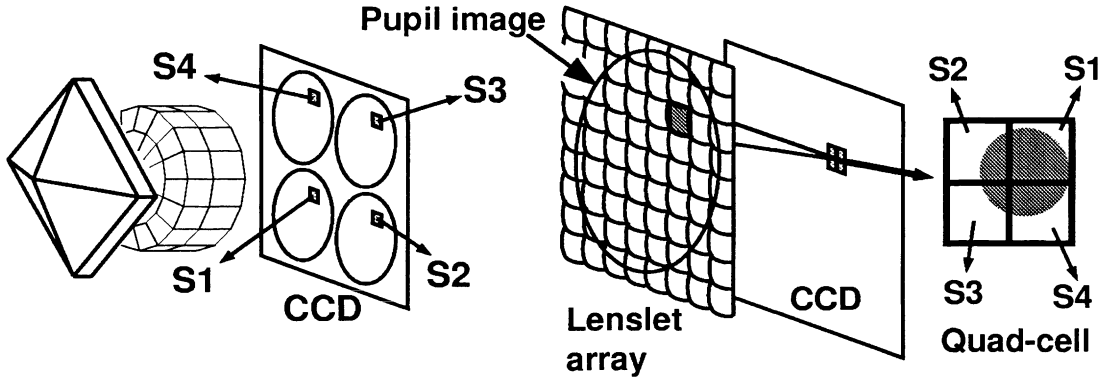

Figure 6. Comparison between the FLWS (on the left) and the Shack-Hartmann (on the right) wavefront sensors. For both the sensors the four detector channels associated to a sensing zone are hilighted

giving $\alpha \approx 5$ deg for $F = 32$ (TNG case) and $n \approx 1.5$. For such a small angle the pyramid operates essentially in normal incidence, reducing the problems associated to the polarization and the chromatic dispersion introduced by the refraction through it. The edge dimension is stated by the diffraction limited FWHM, requiring an edge thickness of a few microns for $F = 32$ in the V band. This specification together with the small angle α bring to a hard work for the pyramid production, because the finite dimension of the grains used to polish the surfaces tends to smooth the edges. M.Ghigo and G.Crimi from the Observatory of Merate (Italy) are working to solve the problems associated to the pyramid manufacturing. They have already produced some preliminary pyramid with $\alpha \approx 6$ deg and 10-20 μm edge thickness. Narrower edges will be produced using super-fine polishing and ion-beam modeling technique.

3. FOUCAULT-LIKE AND SHACK-HARTMANN SENSORS COMPARISON

In Fig. 6 a comparison between the FLWS and the Shack-Hartmann (SH) wavefront sensor is summarized. The two sensors have the following main common characteristics:

- both the sensors give a measurement of the first derivatives of the wavefront;
- they have the same spatial sampling when the pattern of the lenslets on the image of the pupil on the SH array is equal to the pattern of detector channels on each image of the pupil in the FLWS;
- the same integration time T can be obtained providing a tilt modulation of frequency $1/T$ for the FLWS (a frequency $0.5/T$ can be used if the integration start is synchronized with a turning point of the oscillation);

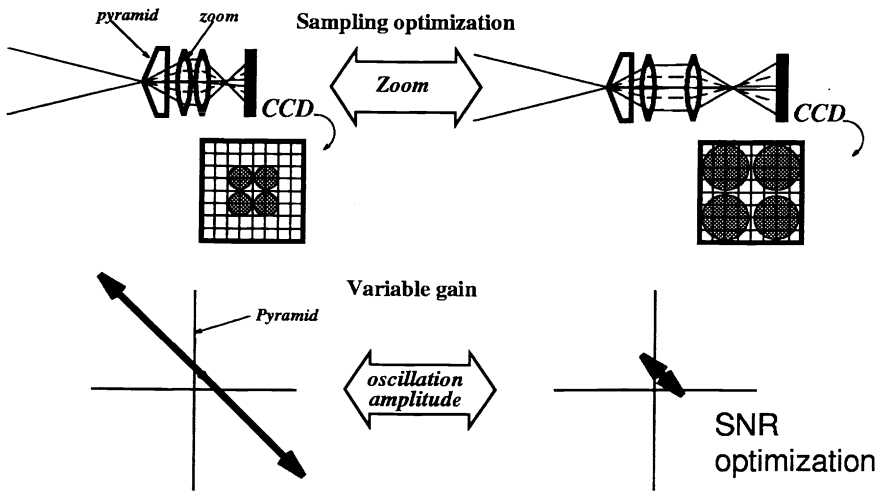

Figure 7. Flexibility of the FLWS. The sensor can change easily the sampling using a zoom lens as relay lens (on the top) and the gain modifying the tilt modulation amplitude (on the bottom). In the bottom figure the SNR is boosted, for instace, reducing the amplitude when the difference beetween the measured signals (see Eq. 3) approach the noise level.

- they use four channels of the detector per sensing zone, a 2x2 square behind a lenslet for the SH and one channel for each pupil image in the FLWS case;
- both the sensors enter a *saturation* regime for the sensing zones where $|\nabla W|$ is greater then the tilt amplitude $\delta\theta$ (in the FLWS case) or then the angular radius of the spot generated by a lenslet (in the SH case);
- they have the same relationships between the signals and the wavefront derivatives, providing the angular tilt amplitude $\delta\theta$ equal to the effective angular radius of the image of the guide star produced by a lenslet of the SH;
- finally, as a consequence of the previous point, both the sensors have the same behavior in terms of noise propagation.

The FLWS, however, has intrinsic advantages respect to the SH that are very useful for adaptive optics applications, as shown in Fig. 7:

- if a zoom lens is used as relay lens, the spatial sampling over the pupil can be easily changed and optimized for the operating wavelength of the adaptive optic system, the status of turbulence and the brightness of the available guide star;
- the gain of the sensor can be optimized while the system operates simply changing the amplitude of the tilt modulation $\delta\theta$. The tilt amplitude can be increased to avoid saturation regime if atmospheric local tilt is too large (during the transient after the adaptive optics system is switched, for instance), or to maintain as higher as possible the signal to noise ratio during the measurements.

The last characteristic is common to the curvature sensor for which the vibrating membrane used to modulate the defocus[1] plays the same role of the tilt modulator in the FLWS. Another advantage is represented by the better data packing respect to the SH, for which unused pixel rows and columns are inserted around each 2x2 channel group used for the sensing in order to avoid crosstalk among them. In the FLWS, for which fixed images of the pupil and not wandering spots are recorded, the "buffer" pixels are not necessary and the detector can be smaller then in the SH case, when the same sampling is provided (about a factor 4 in terms of the number of channel).

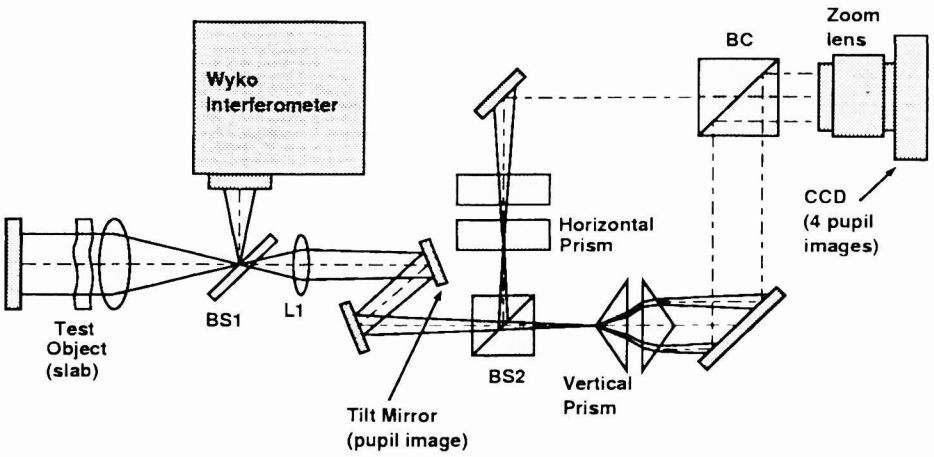

Figure 8. Sketch of the laboratory layout for the FLWS prototype test.

4. THE FLWS PROTOTYPE

4.1. Laboratory layout

In order to demonstrate the feasibility of the FLWS, we developed a laboratory prototype of it. In Fig. 8 the laboratory layout used to compare the static wavefront measurements obtained by the FLWS and a commercial Fizeau interferometer (Wyko) is sketched. A focused He-Ne laser beam is generated by the Wyko interferometer and it is reflected by the beam splitter BS1 towards a collimating lens. After the lens a low optical quality slab (the test object) can be placed in order to be able to change the wavefront aberration to be measure. After a double pass in the test object, the beam is reflected back to the beam splitter BS1 where it is divided in two paths, one goes back to the Wyko for the interferometric measurements of the wavefront and the other one passes through the beam splitter towards the FLWS. The first element of the sensor is the lens L1 that refocuses the beam ($F/117$) and produces a 5 mm image of the test object aperture on the tilt modulator mirror (a Physik Instrumente position controlled tip-tilt mirror). In this prototype a double prism configuration was used instead of a single pyramid: the beam is split before the focal point obtaining two paths where prisms with orthogonal edges are placed on the focal points; the four beams generated by the prisms (two for each path) are recombined and four images of the pupil are produced by a zoom lens on a 8-bit CCD detector. In the described prism-based configuration half the light is lost in the beam recombination process and the use of the pyramid, that doesn't suffer this problem, is fundamental for the final unit.

4.2. Experimental results

In Fig. 9 the effect of tilt modulation is shown. The top figure is acquired while the modulation is switched off. Large dark zones can be noted due to the saturation regime. When the tilt mirror is switched on the dark zones disappear (providing enough large tilt amplitude as stated by Eq. 2) and the sensor enters the linear regime. In our measurements we used a sampling of 120 points along the pupil diameter and a 100 Hz ramp modulation with amplitude $\delta\theta = 0.427 \pm 0.007$ mrad (enough large to avoid the saturation regime for all our measurements). The oscillation was performed at 45 deg respect to the prism edges.

The acquired images of the pupil associated to each prism are superimposed, and the ratio between their difference and sum gives an estimation of the wavefront derivatives (Fig 10, top image) as described in the previous section. The wavefront is obtained using a least-squares modal reconstructor[13] giving the first 26 Zernike coefficients as defined by Noll.[14] In the bottom image of Fig. 10 an example of reconstructed wavefront is shown, together with the difference between the derivatives of the reconstructed and estimated wavefront (the same color scale is used).

The wavefront aberrations measured by the FLWS and the Wyko interferometer are not the same because of the aberrations introduced by the non-common path. Moreover the absolute astigmatism value cannot be estimated by the present configuration of the FLWS prototype because of the uncertainty in the relative focus positioning of the prisms (this problem will be overcome with the use of the pyramid as soon as possible). In order to eliminate the

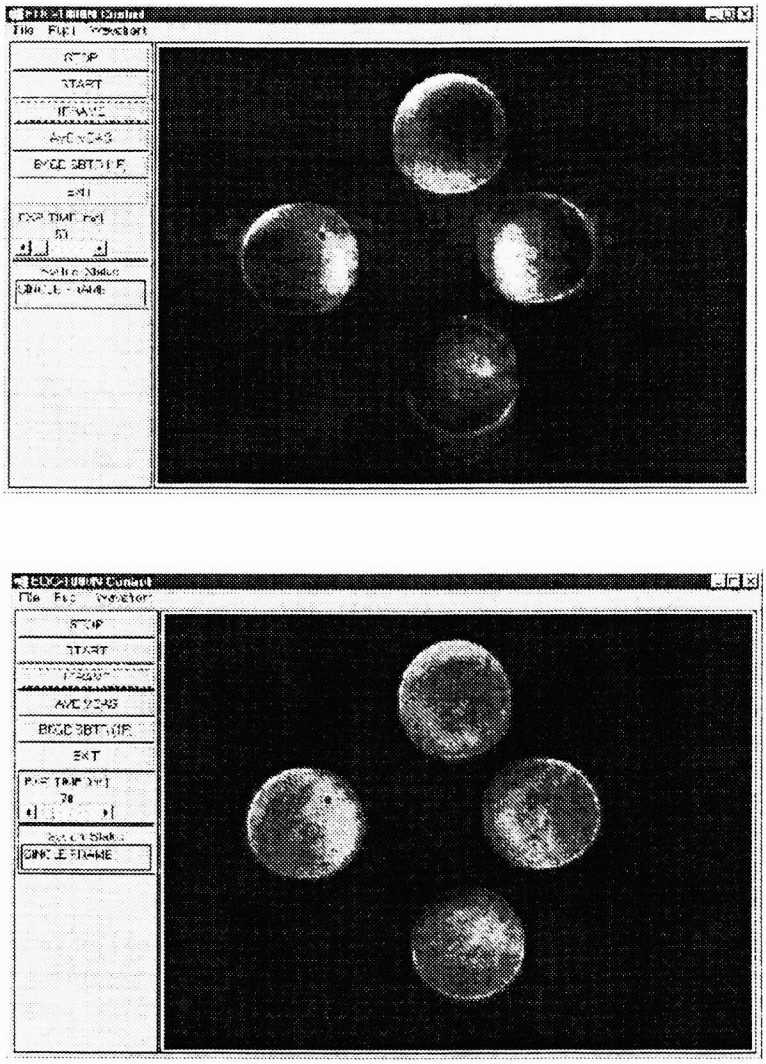

Figure 9. Acquisition of the pupil images. On the top: the tilt modulation is not performed. The sensor is in the saturation regime. On the bottom: the tilt modulation is performed and the whole images of the pupil are illuminated. The sensor operates in the linear regime.

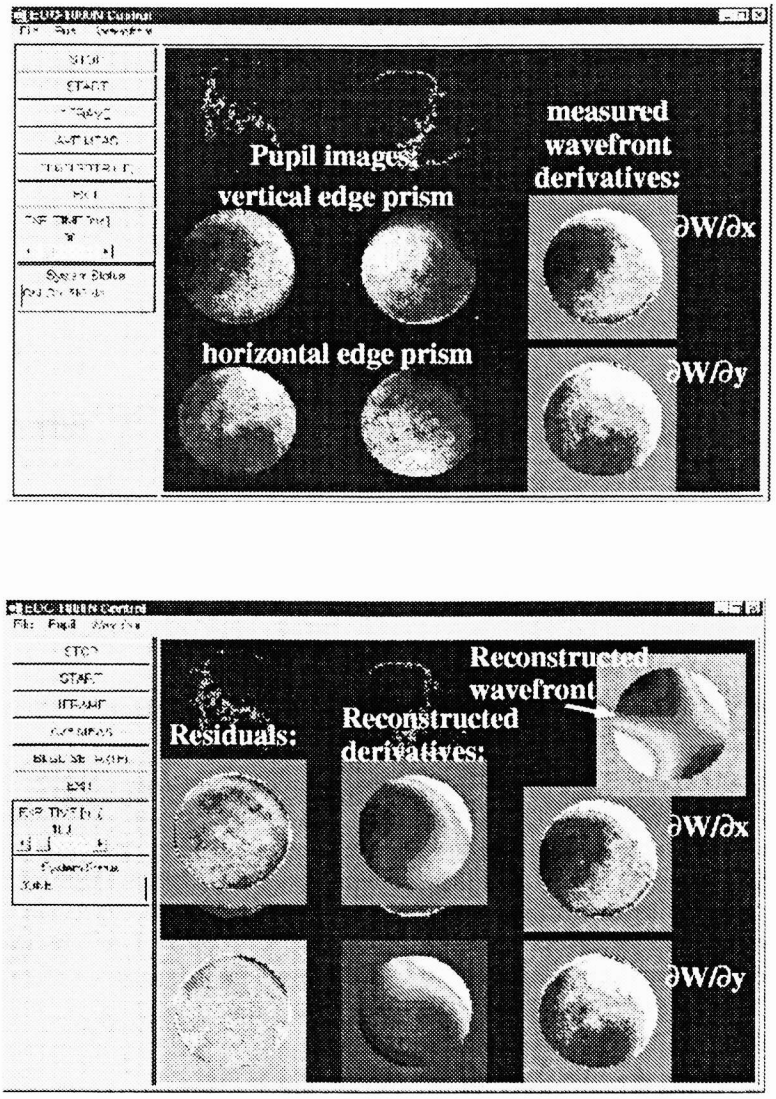

Figure 10. Derivatives estimation from the image pupil (top figure) and wavefront reconstruction (bottom figure). A 120x120 sampling on each image of the pupil and a modal reconstructor (26 Zernike modes) were used.

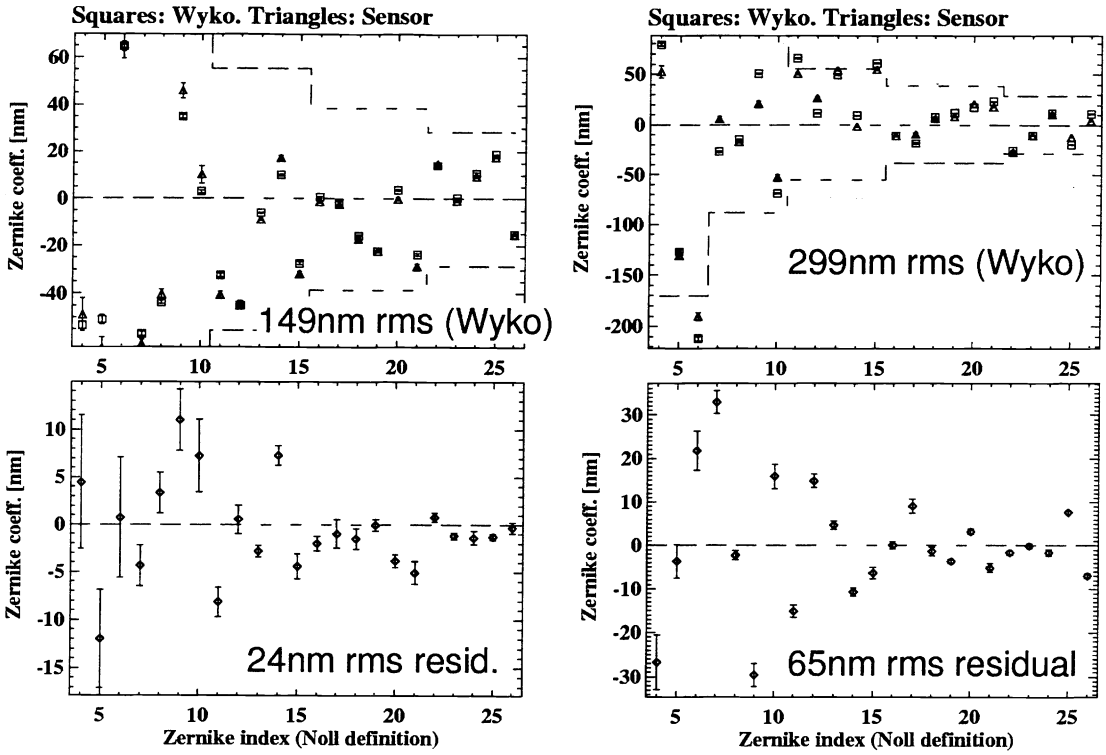

Figure 11. Comparison between the measurements obtained by the FLWS prototype and Wyko interferometer. Two representative results are presented. On the top the measurements and on the bottom the difference between the measurements are reported.

unknown offsets, we performed differential measurements obtained inserting and removing the test slab described in Sec. 4.1.

In Fig. 11 two representative measurements are shown for different test objects. On the top plots the Zernike components measured by the FLWS and the Wyko interferometer are compared. The Wyko measured a 149 nm rms contribution to the wavefront aberrations (for the reported modes) in one case and a 299 nm rms in the other. In both cases the test object was chosen to obtain aberration of the same order of magnitude of the aberrations introduced by the atmospheric turbulence; the dashed lines in the top plots represent the rms values for the Zernike components in the case of a 4m-telescope working in K band with $r_0 = 1$ m. In the bottom plots the difference between the FLWS and Wyko measurements are reported. The FLWS measure differs from the Wyko one of 24 nm rms (16%) in one case and 65 nm rms (22%) in the other case.

5. CONCLUSIONS

The principle of operation of a FLWS has been presented. We showed how the sensor can be considered equivalent to the SH in many aspects: same number of detector channels per sensing zone, same relationships between the recorded signals and the wavefront gradient components and same behavior in terms of noise propagation. Moreover some advantages of the FLWS with respect to the SH has been shown, namely the capability to easily change the spatial sampling over the pupil and the gain during the operation, assuring an optimized behavior of the sensor for different operating conditions.

Finally the developed prototype of the FLWS has been described and the performed static measurements of wavefront aberrations have been presented, showing an error of about 20% in terms of rms respect to the measurements obtained by a commercial Wyko interferometer in the range from 150 to 300 nm rms.

ACKNOWLEDGMENTS

The authors would like to thank F. Rigaut for the useful discussions about the Foucault-like wavefront sensor. This work was partially supported by the CNAA and TMR.

REFERENCES

1. F. Roddier, M. Northcott, and J. E. Graves, "A simple low-order adaptive optics system for near-infrared applications," *Pub. Astr. Soc. Pac.* **103**, pp. 131–149, 1991.
2. R. Ragazzoni, "Pupil plane wavefront sensing with an oscillating prism," *J. Modern Opt.* **43**, pp. 289–293, 1996.
3. R. Ragazzoni, A. Baruffolo, F. Bortoletto, M. D'Alessandro, J. Farinato, A. Ghedina, and E. Marchetti, "Adaptive optics module for tng (adopt@tng): a status report," *Proc. Soc. Photo-Opt. Instrum. Eng.* **2871**, pp. 905–909, March 1997. Provided by the NASA Astrophysics Data System.
4. J. M. Hill, "Large binocular telescope project," *Proc. Soc. Photo-Opt. Instrum. Eng.* **2871**, pp. 57–68, March 1997. Provided by the NASA Astrophysics Data System.
5. P. Salinari, "Large binocular telescope interferometer," *Proc. Soc. Photo-Opt. Instrum. Eng.* **2871**, pp. 564–574, March 1997. Provided by the NASA Astrophysics Data System.
6. P. Salinari and D. Sandler, "High-order adaptive secondary mirrors: where are we?." in this conference: [3353-09].
7. G. Brusa, A. Riccardi, S. Ragland, S. Esposito, C. del Vecchio, L. Fini, P. Stefanini, V. Biliotti, P. Ranfagni, P. Salinari, D. Gallieni, R. Biasi, P. Mantegazza, G. Sciocco, G. Noviello, and S. Invernizzi, "Adaptive secondary p30 prototype: laboratory results." in this conference: [3353-34].
8. R. Biasi and D. Gallieni, "Mmt adaptive secondary prototype development." in this conference: [3353-123].
9. M. Born and E. Wolf, *Principles of optics*, Pergamon, New York, 1985.
10. D. Malacara, *Optical shop testing*, Wiley, New York, 1978.
11. E. Gaviola, "On the quantitative use of the foucault knife-edge test," *J. Opt. Soc. Am.* **26**, pp. 163–169, 1936.
12. D. E. Vandenberg, W. D. Humbel, and A. Wertheimer, "Quantitative evaluation of optical surfaces by means of an improved Foucault test approach," *Optical Engineering* **32**, pp. 1951–1954, 1993.
13. W. H. Southwell, "Wave-front estimation from wave-front slope measurements," *J. Opt. Soc. Am.* **70**, pp. 998–1006, 1980.
14. R. Noll, "Zernike polynomials and atmospheric turbulence," *J. Opt. Soc. Am.* **66**, pp. 207–211, 1976.